PERGAMON

International Journal of Heat and Mass Transfer 45 (2002) 87–98

International Journal of HEAT and MASS TRANSFER

www.elsevier.com/locate/ijhmt

New entrainment rate correlation in annular two-phase flow applicable to wide range of flow condition

Tomio Okawa *, Tsuyoshi Kitahara, Kenji Yoshida, Tadayoshi Matsumoto, Isao Kataoka

Department of Mechanophysics Engineering, Osaka University, 2-1 Yamadaoka, Suita, Osaka 565–0871, Japan

Received 26 July 2000; received in revised form 23 March 2001

Abstract

Assuming the rate of droplet entrainment is characterized by the ratio of the interfacial shear force to the surface tension force acting on the phase interface, new correlation representing the rate of droplet entrainment in annular-dispersed two-phase flow was developed. Although the correlation is based on the simple assumption, the quasi-equilibrium droplet flow rates measured in many experiments were predicted reasonably well (root mean square error of entrainment fraction was roughly halved comparing with several existing correlations). Its applicability to the non-equilibrium situation was also demonstrated by the numerical calculations using a one-dimensional three-fluid model. © 2001 Elsevier Science Ltd. All rights reserved.

1. Introduction

Annular-dispersed two-phase flow is one of the most common flow patterns encountered in nuclear power plants. In this flow regime, the liquid phase flows partly in a liquid film adjacent to the wall surface and partly as droplets in the gas core. In the case of boiling two-phase flows, accurate prediction of liquid phase flow rate in the film is of particular importance since disappearance of the liquid film results in a sudden deterioration of heat transfer from the heating surface, i.e. in the onset of critical heat flux due to dryout; many correlations have been proposed for predicting the flow rate of liquid film or entrained droplets in annular-dispersed two-phase flows. Wicks and Dukler correlated the mass flow rate of droplets in terms of the Martinelli parameter [1]. Using different dimensionless numbers, Paleev and Filippovich [2], Wallis [3] and Ishii and Mishima [4] correlated the entrainment fraction, that is defined by the droplet mass flow rate divided by the total liquid mass flow rate. In these correlations, the flow rate of liquid film or droplets are directly calculated from the flow conditions such as flow rates and thermal properties of the phases and channel geometry. Also, there exists more detailed approach for the same purpose; Govan et al. [5], Sugawara [6,7] and Kataoka and Ishii [8] correlated the rates of deposition and entrainment of droplets per unit time and interfacial area. If these two quantities are known in addition to the droplet flow rate at the inlet, the droplet flow rate at any distance from the inlet can be derived through the integration of balance equation. However, validity of most of the existing correlations has not been tested against the experimental data obtained in wide range of flow condition. Although the correlations developed by Govan et al. are based on a number of data, their entrainment correlation shows considerable scatter. Hence, it can be said that the prediction method of the film flow rate in annular two-phase flow applicable to wide range of flow condition has not been developed in spite of its importance.

In view of these, in the present study, we try to develop a new entrainment rate correlation for accurately predicting the flow rates of liquid film and droplets in annular-dispersed two-phase flow in wide range of flow condition. In the development, assuming the dominant mechanism of droplet entrainment from liquid film into

* Corresponding author. Tel.: +81-6-6879-7257; fax: +81-6-6879-7247.

E-mail address: t-okawa@mech.eng.osaka-u.ac.jp (T. Okawa).

0017-9310/02/$ - see front matter © 2001 Elsevier Science Ltd. All rights reserved.
PII: S0017-9310(01)00111-9

Nomenclature

C	droplet concentration in gas core (kg/m^3)
D	tube diameter (m)
E	entrainment fraction
E_1	entrainment fraction calculated by Eq. (14)
E_∞	equilibrium entrainment fraction
f	friction factor
$f(E_\infty)$	function of E_∞ defined in Eq. (14)
J	volumetric flux (m/s)
J_g^*	dimensionless gas flux
J_{gc}^*	dimensionless gas flux at transition to annular flow
k	mass transfer coefficient (m/s)
k_s	hydrodynamic equivalent wave roughness (m)
k_{E0}	tentative value of entrainment mass transfer coefficient used in Eq. (14) (m/s)
m_D	deposition rate (kg/m^2 s)
m_E	entrainment rate (kg/m^2 s)
n	some power of density ratio
P	pressure (Pa)
R	dimensionless number defined by Eq. (14)
Re	Reynolds number
Sc	Schmidt number
u	cross-sectional area-averaged velocity (m/s)
We	Weber number
w	mass flux (kg/m^2 s)
x_g	quality

Greek symbols

Δh_{eq}	hydrodynamic equivalent wave height (m)
δ	film thickness (m)
λ_E	coefficient defined in Eq. (14)
μ	viscosity (Pa s)
π_E	dimensionless number defined by Eq. (2)
ρ	density (kg/m^3)
σ	surface tension (N/m)
τ	shear force (N/m)
ω	parameter of linear interpolation

Subscripts

cal	calculated value
D	deposition
E	entrainment
e	entrained droplet
f	liquid film
g	gas phase
i	interface
l	liquid phase
max	maximum
w	wall

gas core flow is the shearing-off of roll wave crests, the entrainment rate is correlated in terms of the dimensionless number given as the ratio of interfacial shear force to the retaining force of surface tension acting on the phase interface. In evaluating the surface tension force, the radius of curvature of the phase interface is supposed to be proportional to the thickness of the liquid film, that is estimated from the force balance between the interfacial shear force and wall friction force acting on the liquid film. Since several assumptions are needed in developing the correlation, its validity is tested against the available experimental data.

2. Correlation of droplet entrainment

2.1. Basis of the model

The interfacial structure between gas core and liquid film in annular two-phase flow is extremely complex; a variety of mechanisms of droplet entrainment is described in the literature [9,10]. However, in most flow conditions of interest, the phenomenon dominating the droplet formation process at the phase interface is considered to be the shearing-off of roll wave crests by the turbulent gas flow: the tips of roll waves are drawn out by the interfacial shear force against the retaining force of surface tension, then, the portions of waves are broken up into a number of small atomized droplets. This idea could be supported by the fact that the criterion for the droplet entrainment measured in many experiments are reasonably correlated based on this concept [10]. In addition, it has been pointed out by several researchers that the amount of droplets in equilibrium situation increases with the increase of the interfacial shear force and it decreases with the increase of liquid surface tension [4,11]. From these results, we are led to suppose that the deformation of the phase interface and the rate of droplet entrainment are controlled by the two competing forces, namely, the interfacial shear force exerted by the streaming gas flow promotes the droplet entrainment, while the surface tension force restrains it. Thus, it is assumed in our model that the rate of droplet entrainment is characterized by the following dimensionless number π_E, that is obtained by dividing the interfacial shear force by the retaining force of surface tension

$$\pi_E = \frac{f_i \rho_g J_g^2 \delta}{\sigma}, \tag{1}$$

where f_i is the interfacial friction factor, ρ the density, J the volumetric flux, δ the average film thickness, σ the surface tension and the subscript g denotes the gas phase; in evaluating the interfacial shear force and the

surface tension force in the above equation, it is assumed that the gas velocity is sufficiently larger than the film velocity and the radius of curvature of roll wave is proportional to the average film thickness δ. Next, since the deformation of the phase interface is supposed to be governed by the interfacial shear force and the surface tension force, we adopt the simple assumption that the volume of the entrained droplets is approximately proportional to the dimensionless number π_E:

$$\frac{m_E}{\rho_l} \propto \pi_E, \tag{2}$$

where ρ_l is the liquid density and m_E the mass of the entrained droplets per unit time and per unit interfacial area. It is however considered that the existence of many droplets in gas core also affects the entrainment rate since it modifies the flow structure of gas phase. It is hence expected that the better correlation is to be derived if the effect of droplets is appropriately included. Although the effect of droplets would depend on several parameters such as droplet concentration and droplet size, only the effect of increased inertia of gas core flow due to entrained droplets is simply taken into account by using the density ratio of gas and liquid phases, referring the successful work done by Ishii and Mishima [4]. Using these assumptions, we define the mass transfer coefficient relevant to the droplet entrainment k_E by

$$m_E = k_E \rho_l \pi_E \left(\frac{\rho_l}{\rho_g}\right)^n. \tag{3}$$

Since the above expression for m_E is derived from the assumed hypotheses, its validity is tested against the available experimental data of equilibrium entrainment fraction after several constitutive equations are prepared.

2.2. Constitutive equations

For calculating m_E from Eqs. (1) and (3), constitutive equations of f_i, δ, n and k_E are needed. First, the correlation proposed by Wallis [12] is adopted for estimating f_i:

$$f_i = 0.005\left(1 + 300\frac{\delta}{D}\right), \tag{4}$$

where D is the tube diameter. Next, δ is calculated from the force balance between the interfacial shear force and the wall friction force acting on liquid film:

$$f_i \rho_g u_g^2 = f_w \rho_l u_f^2, \tag{5}$$

where u is the cross-sectional area-averaged velocity, f_w the wall friction factor and the subscript f the liquid film; the effect of gravity is neglected assuming sufficiently thin liquid film. Since the liquid film is thin, u_g and u_f are approximated by

$$u_g \approx J_g, \tag{6}$$

$$u_f \approx \frac{D}{4\delta} J_f. \tag{7}$$

Substituting the above equations into Eq. (5), δ is estimated by

$$\delta \approx \frac{1}{4}\sqrt{\frac{f_w \rho_l}{f_i \rho_g}}\frac{(1-E)J_l}{J_g} D, \tag{8}$$

where E is the entrainment fraction defined by $E = J_e/J_l$ (the subscript e denotes the entrained droplets). The following expression based on Wallis [12] is used for evaluating f_w:

$$f_w = \max\left(\frac{16}{Re_f}, 0.005\right), \tag{9}$$

where Re_f is the film Reynolds number defined by

$$Re_f = \frac{\rho_l J_f D}{\mu_l}, \tag{10}$$

where μ the viscosity. Finally, the correlations for k_E and n are derived from the experimental data of E measured in quasi-equilibrium region of annular two-phase flow. It is known that the droplet flow rate does not vary so much at sufficiently downstream from the inlet if there is no phase change [9], which implies that m_E is almost comparable with the deposition rate of droplet m_D in this region:

$$m_E \approx m_D. \tag{11}$$

Usually, m_D is assumed to be proportional to the droplet concentration in gas core C:

$$m_D = k_D C, \tag{12}$$

where k_D is the mass transfer coefficient of droplet deposition. Assuming the relative velocity between gas phase and droplets is negligible comparing with the gas phase velocity, C is approximated by

$$C \approx E\rho_l \frac{J_l}{J_g}. \tag{13}$$

Substitution of Eqs. (1), (3), (8), (12) and (13) into Eq. (11) yields

$$f(E_\infty) \equiv \frac{E_\infty}{1-E_\infty} = \frac{1}{4}\frac{k_E}{k_D}\frac{\sqrt{f_i f_w}\sqrt{\rho_g \rho_l} J_g^2 D}{\sigma}\left(\frac{\rho_l}{\rho_g}\right)^n = \lambda_E R \quad (k_E = \lambda_E k_{E0}), \tag{14}$$

where E_∞ is the entrainment fraction in equilibrium situation. Since the value of k_E is unknown, the tentative value is used for calculating the dimensionless number R. In the above equation, this value is denoted by k_{E0} and it is set at 1 m/s. Consequently, if the correlation of k_D is given, the values of $f(E_\infty)$ and R in each

experiment can be calculated from the measured value of E_∞. Furthermore, if the coefficient λ_E is reasonably correlated from the relation between R and $f(E_\infty)$, one can finally obtain the correlation for k_E.

For calculating k_D, we try to use the correlation that is applicable to wide range of flow condition. Govan et al. plotted the relationship between the dimensionless deposition mass transfer coefficient $k_D\sqrt{\rho_g D/\sigma}$ and the dimensionless droplet concentration C/ρ_g for a large number of experimental data. Using this result, it has been pointed out that the mass transfer coefficient of droplet deposition decreases with the increase of droplet concentration and the correlation shown in Eq. (A.4) has been proposed [5]. Although their original correlating line is discontinuous as shown in the equation, considerable scattering still exists in their result and the indicated discontinuity seems obscure. For this reason, giving priority to capturing the overall trend in the present study, the following single correlating line is adopted for calculating k_D:

$$k_D\sqrt{\frac{\rho_g D}{\sigma}} = 0.0632\left(\frac{C}{\rho_g}\right)^{-0.5}. \tag{15}$$

Since the data have shown considerable scattering, it is clear that further improvement of the correlation for k_D is still required. However, the above correlation is as accurate as the original one and it can predict approximately two-thirds of the large and varied experimental data within the error of ±30%.

Now, the relation between the dimensionless number R and the function $f(E_\infty)$ is investigated for the 17 experimental data sets of equilibrium entrainment fraction to derive the correlation for k_E. The range of main flow parameters used in each data set are summarized in Table 1 [13–24]. It is however noted that the accuracy of the entrainment rate correlation would be deteriorated if the data obtained in the flow pattern other than annular flow are included in the data sets. For this reason, only the data that are surely obtained in annular flow condition are used. There are several methods to determine the transition to annular flow, and one of the simplest methods is shown below:

$$J_g^* = J_g\sqrt{\frac{\rho_g}{gD(\rho_l-\rho_g)}} > J_{gc}^*, \tag{16}$$

where J_{gc}^* is the dimensionless gas flux at the transition and several values around unity are recommended in the literature [9,12]. However, since there exists transition regime between slug or churn flow and annular flow, the value of 2 is used for J_{gc}^* to surely exclude the undesirable data. As a result, 1032 data are selected from the 1083 data in total. At the present time, the effect of droplets on entrainment rate has not been well understood, but these data are satisfactorily correlated if the value of 0.2 is used for n. For this reason, this value is used for calculating R. The relation between R and the function $f(E_\infty)$ are plotted in Fig. 1. As shown in the figure, the values of $f(E_\infty)$ measured in most experimental conditions are reasonably correlated by

$$f(E_\infty) = \lambda_E R = 1.85\times10^{-4}R^{1.06}. \tag{17}$$

However, if the results are carefully investigated, it is found that large discrepancies are seen in the results for the low-pressure steam–water data of high quality. One of the main reasons of the discrepancy is thought to be the correlation used for k_D, since the experimental datum of k_D obtained in low-pressure steam–water flow is scarce

Table 1
Sources of entrainment fraction data

Ref.	Fluids	D (mm)	P (MPa)	w (kg/m^2 s)	x_g (%)	No. of data
1. Cousins et al. [13]	Air–water	9.5	0.12–0.27	80–530	15–93	52
2. Cousins and Hewitt [14]	Air–water	9.5	0.14–0.25	159–877	8–69	434
3. Cousins and Hewitt [14]	Air–water	31.8	0.20–0.21	107–199	46–81	24
4. Hewitt and Pulling [15]	Steam–water	9.30	0.24–0.45	297	14–76	66
5. Yanai [16]	Steam–water	12.0	0.34	139–278	11–80	20
6. Wurtz [17]	Steam–water	10.0	3.0–9.1	500–3000	8–60	71
7. Wurtz [17]	Steam–water	20.0	7.1	500–2000	20–70	20
8. Keeys et al. [18]	Steam–water	12.7	3.5–6.9	1300–2740	15–69	21
9. Nigmatulin et al. [19]	Steam–water	13.3	0.91–10.0	500–4000	10–75	46
10. Whalley et al. [20]	Air–water	31.8	0.12–0.35	79–792	10–91	117
11. Whalley et al. [20]	Air–trichlorethane	31.8	0.27–0.28	158–319	35–90	16
12. Singh et al. [21]	Steam–water	12.5	6.9	271–963	28–93	28
13. Bennet et al. [22]	Steam–water	9.3	0.38	297	20–80	12
14. Owen et al. [23]	Air–water	31.8	0.24	120–550	17–82	47
15. Asali [24]	Air–water	22.9	0.10	53–257	25–92	25
16. Asali [24]	Air–water	42.0	0.10	54–188	30–93	25
17. Asali [24]	Air–glycerin	42.0	0.10	73–182	36–85	8

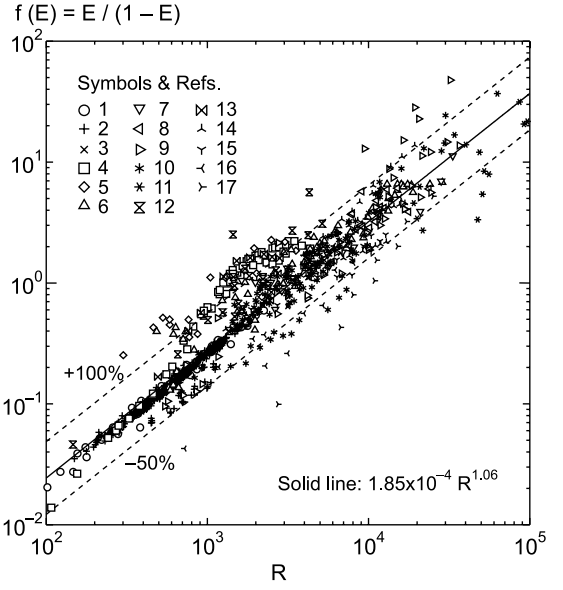

Fig. 1. Relation between the dimensionless number R and the function $f(E)$ (deposition mass transfer coefficient is calculated from Eq. (15)). For reference numbers 1–17 see Table 1.

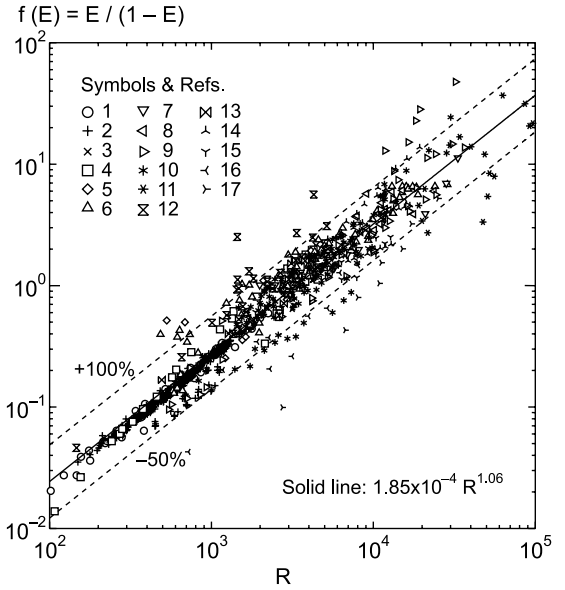

Fig. 2. Relation between the dimensionless number R and the function $f(E)$ (deposition mass transfer coefficient is calculated from Eqs. (15) and (18)). For reference numbers 1–17 see Table 1.

[16]. For this reason, it is tested if better result can be obtained by using another correlation for k_D in this condition. There exist a number of correlations for k_D, but the following correlation proposed by Sugawara [6,7] is selected since his correlation has been mainly applied to the prediction of steam–water two-phase flow.

$$\frac{k_D}{u_g} = 0.009\left(\frac{C}{\rho_g}\right)^{-0.5} Re_g^{-0.2} Sc^{-2/3}, \tag{18}$$

where Re_g and Sc are the gas phase Reynolds number and the Schmidt number, respectively. Note that the above correlation is used only for the low-pressure steam–water data of high quality. If the deposition mass transfer coefficients calculated by Eqs. (15) and (18) are denoted by k_{D15} and k_{D18}, respectively, the method for calculating k_D adopted here is summarized as follows:

$$k_D = \omega k_{D15} + (1-\omega)k_{D18} \tag{19}$$

- fluids are not steam–water: $\omega = 1$
- steam–water flow
  $10^{-6}P > 1$ or $x_g < 0.2$: $\omega = 1$,
  $10^{-6}P < 0.5$ and $x_g > 0.25$: $\omega = 0$,
  $0.2 < x_g < 0.25$ and $10^{-6}P < -10x_g + 3$:
  $\omega = 5 - 20x_g$ (linear interpolation),
  $10.5 < 10^{-6}P < 1$ and $10^{-6}P > -10x_g + 3$:
  $\omega = 2 \times 10^{-6}P - 1$ (linear interpolation).

where x_g is the quality andω denotes the parameter to linearly interpolate the two correlations. Adopting this treatment, the measured $f(E_\infty)$ is reasonably correlated by Eq. (17) as demonstrated in Fig. 2.

Finally, comparison of Eqs. (14) and (17) reveals that the correlation of k_E is given by

$$k_E = 1.85 \times 10^{-4} R^{0.06}. \tag{20}$$

As shown in the above correlation, the value of k_E defined by Eq. (3) is not affected by the flow condition so much, although there is slight dependence on the dimensionless number R. This result suggests that the rate of droplet entrainment m_E is adequately described by the simple expression of Eq. (3) in wide range of flow condition shown in Table 1.

3. Comparison with data

3.1. Entrainment fraction in quasi-equilibrium region

Since $f(E_\infty)$ is reasonably correlated as the function of R as shown in Fig. 2, one can expect that not only $f(E_\infty)$ but E_∞ itself is also reasonably predicted by the same manner. It is however noted that the dimensionless number R is the function of E_∞ and the measured value of E_∞ is used for calculating R in Fig. 2. Hence, accuracy of Eq. (14) is not readily understood from the figure. For this reason, the value of E_∞ calculated from Eq. (14) is directly compared with the measured entrainment fraction.

If the constitutive equations of f_i, f_w, k_D and k_E given in the previous chapter are substituted into Eq. (14), the

entrainment fraction in quasi-equilibrium region E_∞ is estimated. Since f_i and f_w are the functions of E, an iterative calculation is needed in estimating E_∞. It is experimentally observed by several researchers that no more entrainment occurs if Re_f is smaller than the critical film Reynolds number Re_{fc} [5,23,24]. The maximum possible entrainment fraction E_{max} is therefore given by:

$$E_{max} = 1 - \frac{J_{fc}}{J_l} = 1 - \frac{\mu_l Re_{fc}}{\rho_l J_l D}. \quad (21)$$

This fact is interpreted that the roll wave is not formed if $Re_f < Re_{fc}$. However, in the model presented in the previous chapter, the existence of roll wave whose radius of curvature is proportional to δ is assumed on the phase interface. It is hence expected that the present model overestimates the droplet flow rate when the liquid phase volumetric flux is very small. For simply taking into account the above experimental observation, the predicted entrainment fraction E_{cal} is set at E_{max} if the calculated result from Eq. (14) E_1 is greater than E_{max}:

$$E_{cal} = \min(E_1, E_{max}). \quad (22)$$

Referring to the existing correlations [5,24], the value of Re_{fc} is assumed to be 320.

Comparative representations of measured and predicted entrainment fractions in quasi-equilibrium region are shown in Fig. 3(a). As indicated in the figure, the present method predicts the measured entrainment fractions within the error of ± 0.15 with small number of exceptions. To elucidate the performance of the present method, the predicted results with the three widely used correlations [4–7] are shown in Figs. 3(b)–(d), respectively, and the mean error and the root mean square error of E_{cal} in each correlation are summarized in Table 2. The details of the existing three correlations are described in Appendix A. From Fig. 3, several features of the correlations are recognized. Ishii's correlation predicts the entrainment fraction of air–water annular flow in small diameter tube quite well, but the accuracy for the air–water annular flow in larger diameter tube is worse to some extent. If it is applied to the steam–water flow, it underestimates the small entrainment fraction and overestimates the large entrainment fraction. Since it underestimates the film flow rate when the entrainment fraction is large, it would be one of the choices in order to safely avoid the occurrence of dryout in engineering plants. Govan's correlation shows reasonably good agreement with large portion of the data, but it overestimates the entrainment fraction of air–water flow in small diameter tube and underestimates that of steam–water flow when the gas flow rate is small. Sugawara's correlation is quite good for the steam–water data except those given by Singh et al., but it would not be applicable to the air–water flow. Comparing with these existing correlations, the present correlation gives generally better results for all the data tested. As shown in Table 2, the root mean square error of the predicted entrainment fraction of the present correlation is roughly half of those of the other three correlations. Furthermore, it was separately confirmed that these existing correlations give better predictions than several older correlations [2,3,25], and Govan et al. [5] demonstrated that their correlation predicts the droplet concentration with higher accuracy than some other correlations. It is hence expected from the above analysis that the present correlation can contribute to the improvement of prediction method of liquid film or droplets flow rate in annular-dispersed two-phase flow.

3.2. Droplet flow rate in non-equilibrium region

Since it was demonstrated in the previous section that the present correlation predicts the equilibrium entrainment fraction with higher accuracy than the existing ones, its applicability to the non-equilibrium or developing flows is tested. For this purpose, the present correlation was incorporated into the computer program, ANDRE, which is based on a one-dimensional multi-fluid model [26]. Its details are described in Appendix B. It is noted that k_E is basically calculated by Eq. (20), but it is set at zero when $Re_f < Re_{fc}$.

The computer program is applied to the experiments of annular two-phase flow in a vertical round tube conducted by Cousins et al. [13]. They introduced water into air flow through a porous sinter injector whose inner diameter equaled to the tube diameter, and measured the film flow rate at 10 elevations from the injector by blowing off the film. All the liquid flows as a liquid film adjacent to the wall surface just above the injector ($z = 0$), and droplet flow rate gradually increases with elevation due to the droplet entrainment. The comparisons of the predicted droplet flow rates with all the experimental data given in their paper are shown in Figs. 4(a)–(d), and the comparative representations of predictions and measured data are given in Fig. 5. As shown in these figures, the present model gives generally good agreement with the data, which would demonstrates that the present correlation is applicable not only to quasi-equilibrium but also to non-equilibrium situations. However, Fig. 5 indicates that the present model considerably overestimates the droplet flow rate when its value is very small; the reason of the error is investigated. Hewitt and Hall-Taylor have pointed out that roll wave may take a finite distance along the channel to grow and longer distance is required particularly at low film flow rate [9]. It is hence probable that roll wave is not created and no droplet is entrained within a finite distance from the injector. This phenomenon is clearly seen in Fig. 6: nonzero droplet flow rates are measured at the most upstream measuring point at higher liquid flow rates, while no droplets are measured within a finite distance at lower liquid flow rates. On the other hand,

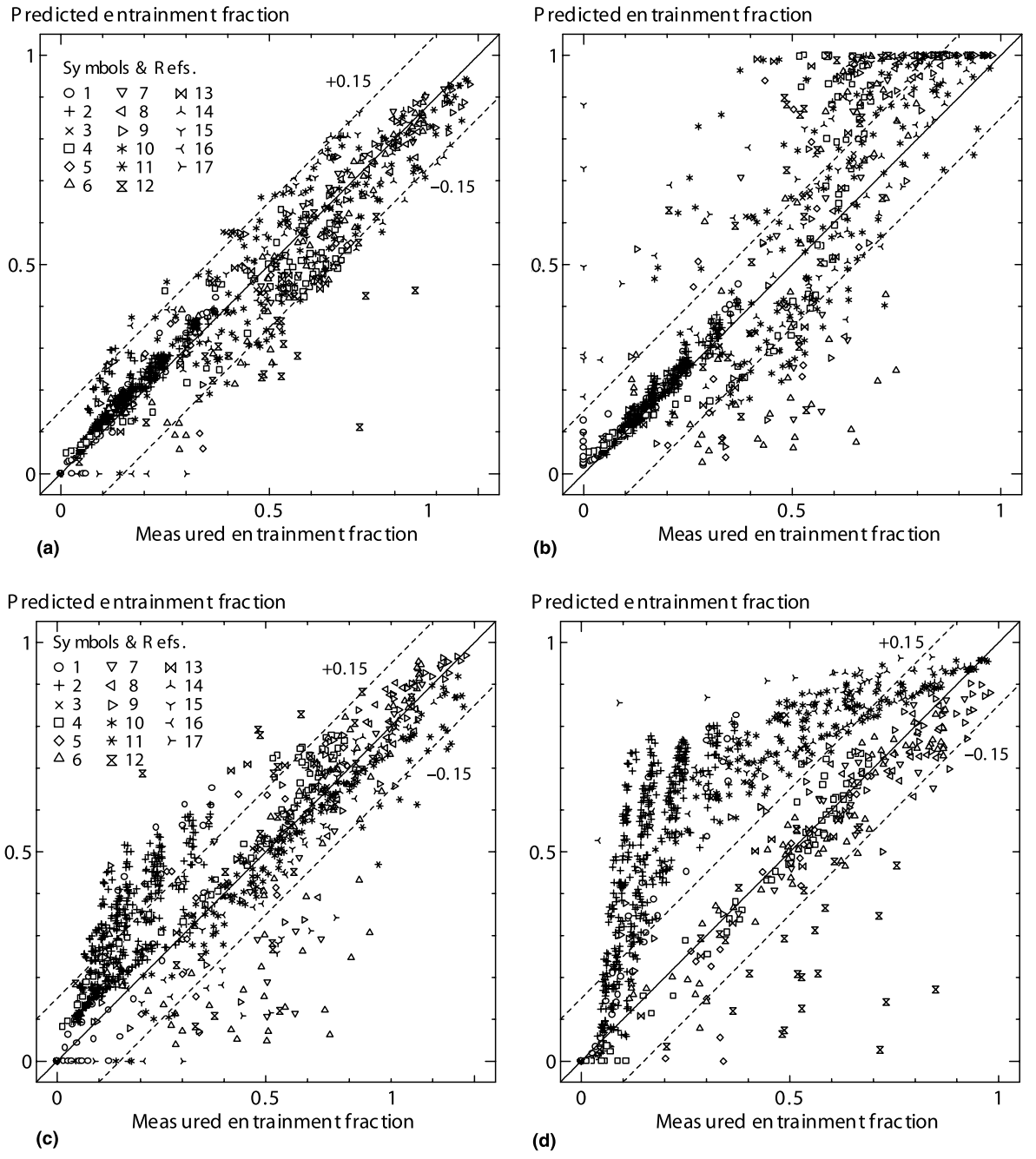

Fig. 3. Comparative representations of measured and predicted entrainment fraction in quasi-equilibrium region. (a) Present correlation. (b) Ishii and Mishima [4]. (c) Govan et al [5]. (d) Sugawara [6,7]. For reference numbers 1–17 see Table 1.

since this length effect is not taken into account in the present model (it assumes the existence of roll wave whose radius of curvature is proportional to the film thickness), the increase of droplet flow rate is seen just above the injector as indicated with solid lines in the figure. This is the primary reason of the discrepancy seen in Fig. 5. However, since experimental information on the length effect is scarce and it would depend on the injection method, reliable correlation for this effect has not been developed. Thus, the error of the predicted droplet flow rate could be greater when the flow rate of liquid phase is very small. However, since the liquid flow

Table 2
Performance of several correlations in predicting entrainment fraction (mean error and root mean square error)

Correlation	Air–water data	Steam–water data	All data
Present correlation	0.016/0.066	−0.046/0.108	−0.003/0.081
Ishii and Mishima [4]	0.031/0.121	0.064/0.223	0.041/0.156
Govan et al. [5]	0.081/0.136	−0.003/0.152	0.051/0.142
Sugawara [6,7]	0.276/0.318	−0.037/0.127	0.142/0.278

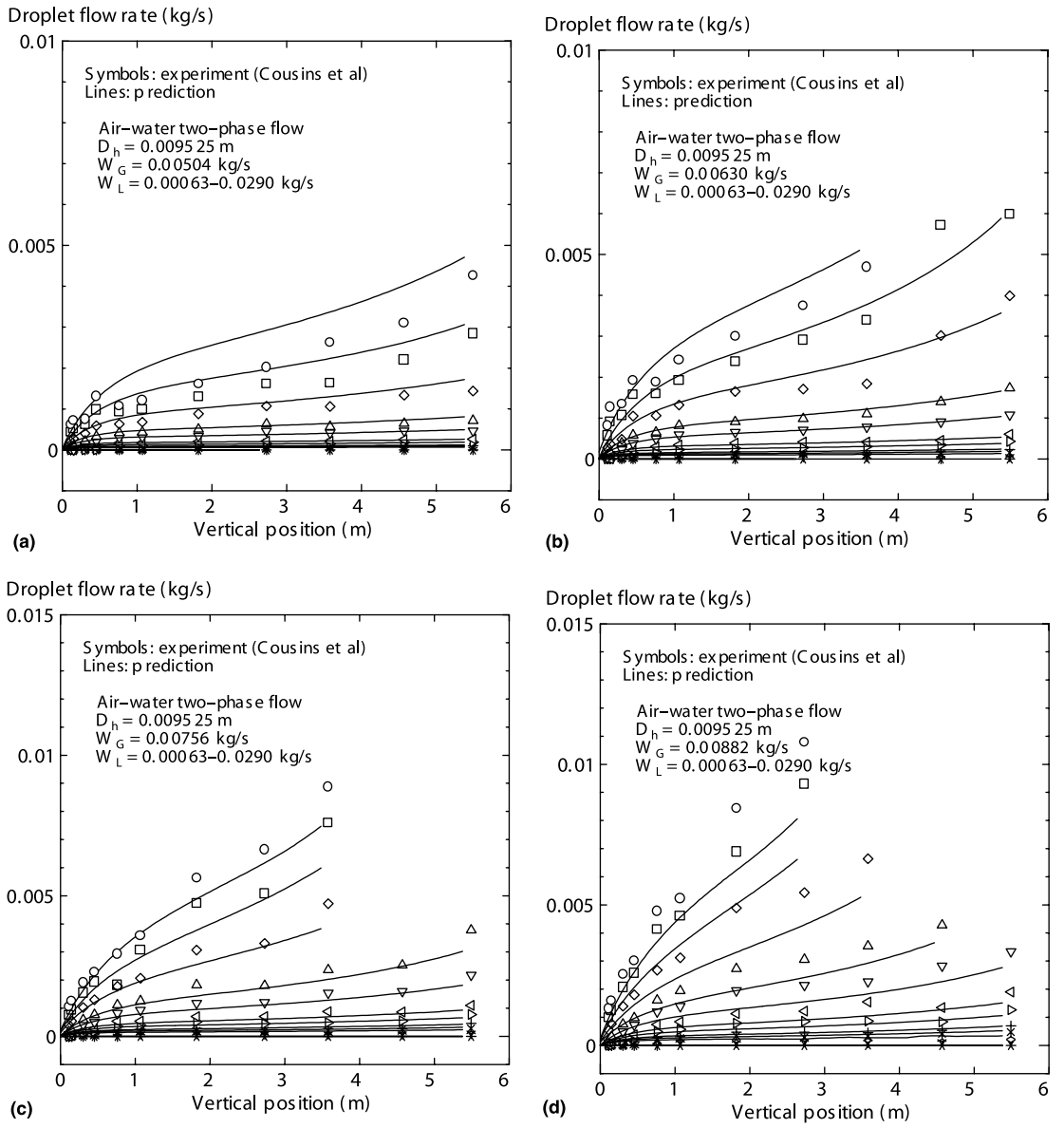

Fig. 4. Comparisons of predicted and measured droplet flow rates in air–water annular two-phase flow in non-equilibrium conditions. (a) $w_g = 5.04 \times 10^{-3}$ kg/s. (b) $w_g = 6.30 \times 10^{-3}$ kg/s. (c) $w_g = 7.56 \times 10^{-3}$ kg/s. (d) $w_g = 8.82 \times 10^{-3}$ kg/s.

rate gradually decreases along the flow channel in the case of boiling two-phase flow, the length effect would not be a significant problem in the prediction of dryout. For this reason, to test the performance of the present model to predict the rate of droplet entrainment itself, the nonzero droplet flow rate obtained at the most

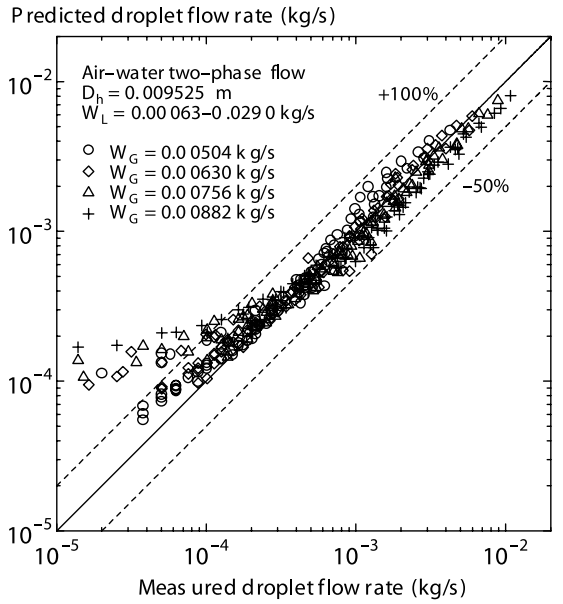

Fig. 5. Comparative representations of predicted and measured droplet flow rates in non-equilibrium situation (droplet flow rate is set at 0 kg/s as the inlet boundary condition).

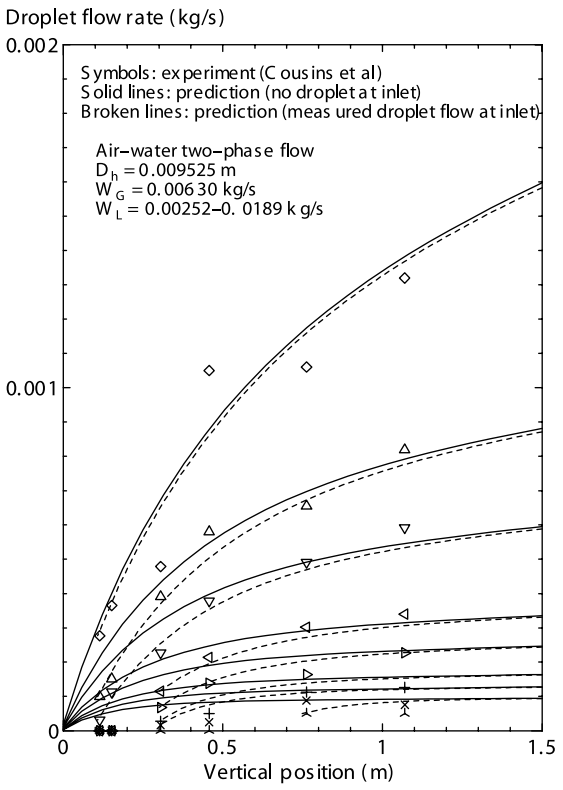

Fig. 6. Droplet flow rates just above the injector (length effect on the onset of entrainment).

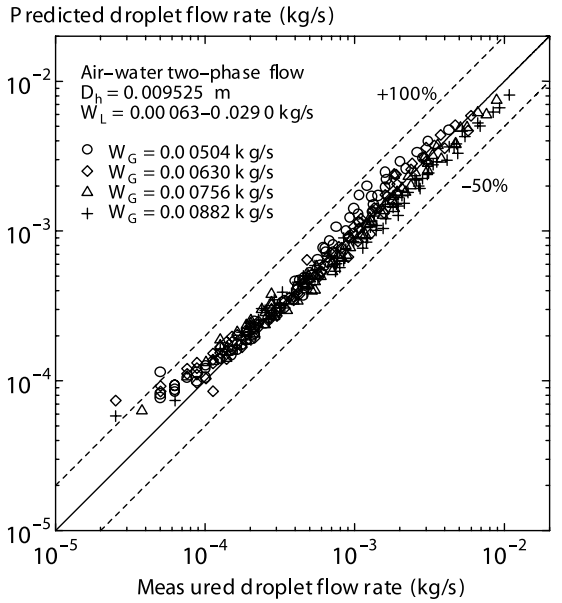

Fig. 7. Comparative representations of predicted and measured droplet flow rates in non-equilibrium situation (nonzero droplet flow rate obtained at the most upstream measuring point is used as the inlet boundary condition).

upstream measuring point in each experimental condition is used as the inlet condition of the analysis. Typical examples of the calculated droplet flow rate in this case are shown with broken lines in Fig. 6 and the comparative representations are given in Fig. 7. As demonstrated in these figures, the predicted results in non-equilibrium situation reasonably agree with the measured data in this analytical condition. This results would confirm that the rate of droplet entrainment is satisfactorily predicted by the present model even in the non-equilibrium situations.

4. Summary and conclusions

New entrainment rate correlation was proposed for accurately predicting the flow rates of liquid film and droplets in annular-dispersed two-phase flow. The correlation is based on the simple assumption that the rate of droplet entrainment is approximately proportional to the ratio of the interfacial shear force to the retaining force of surface tension acting on the phase interface. For evaluating the two forces and the proportionality factor, the additional correlations of the interfacial and wall friction factors and the mass transfer coefficients of droplet deposition and entrainment were required. In the present study, reliable correlations were adopted for the friction factors and the deposition mass transfer coefficient and new correlation was developed for the entrainment mass transfer coefficient using available

experimental data of quasi-equilibrium entrainment fraction measured in vertical round tube.

Validity of the present correlation was tested against 17 experimental data sets of annular two-phase flow in which the data of air–water, low-pressure steam–water, high-pressure stem-water, air–trichlorethan and air–glycerin two-phase flows were included. The predicted results of quasi-equilibrium entrainment fraction were agreed with the most data tested within the error of ± 0.15; the root mean square error was roughly half of those of the several widely used correlations. Furthermore, incorporating the new correlation into the computer program based on a one-dimensional three-fluid model, its applicability to non-equilibrium situation was confirmed. It is hence expected that the present correlation enables more accurate prediction of the liquid film or droplets flow rates in annular-dispersed two-phase flow. It is however noted that the agreement with the data was not satisfactory in some experiments. Clearly, further improvements of the correlations representing the interfacial and wall friction forces and the deposition and entrainment rates of droplets are required for more accurate prediction.

Appendix A. Summaries of the existing correlations

The outlines of the methods for calculating E_∞ from the three correlations [4–7] are described. First, Ishii and Mishima directly correlated E_∞ as follows:

$$E_\infty = \tanh(7.25 \times 10^{-7} We^{1.25} Re_l^{0.25}), \tag{A.1}$$

where the liquid phase Reynolds number Re_l and the effective Weber number We are defined by:

$$Re_l = \frac{\rho_l J_l D}{\mu_l}, \tag{A.2}$$

$$We = \frac{\rho_g J_g^2 D}{\sigma}\left(\frac{\rho_l - \rho_g}{\rho_g}\right)^{1/3}. \tag{A.3}$$

Next, in the method of Govan et al. [5], the deposition mass transfer coefficient and the rate of droplet entrainment are correlated:

$$k_D\sqrt{\frac{\rho_g D}{\sigma}} = \min\left[0.18, 0.083\left(\frac{C}{\rho_g}\right)^{-0.65}\right], \tag{A.4}$$

$$\frac{m_E}{w_g} = 5.75 \times 10^{-5}\left[(w_f - w_{fc})^2 \frac{D\rho_l}{\sigma\rho_g^2}\right]^{0.316} \tag{A.5}$$

for $w_f > w_{fc}$,

$$\frac{w_{fc} D}{\mu_l} = \exp\left[5.8504 + 0.4249\frac{\mu_g}{\mu_l}\sqrt{\frac{\rho_l}{\rho_g}}\right], \tag{A.6}$$

where w is the mass flux and μ is the viscosity. If Eqs. (12), (13) and (A.4) are used, m_D is expressed in terms of E. Since w_f is the function of w_l and E, m_E is also expressed in terms of E. Substitution of these expressions of m_D and m_E into Eq. (11) yields the equation about E_∞, which is iteratively solved for estimating E_∞.

Finally, in the method of Sugawara [6,7], the deposition mass transfer coefficient and the rate of droplet entrainment are correlated by

$$\frac{k_D}{u_g} = 0.009\left(\frac{C}{\rho_g}\right)^{-0.5} Re_g^{-0.2} Sc^{-2/3}, \tag{A.7}$$

$$m_E = 1.07\left(\frac{\tau_{fg}\Delta h_{eq}}{\sigma}\right)\left(\frac{u_g\mu_l}{\sigma}\right)\left(\frac{\rho_l}{\rho_g}\right)^{0.4}, \tag{A.8}$$

where

$$\tau_{fg} = \frac{f_i}{2}\rho_g(u_g - u_f)^2, \tag{A.9}$$

$$f_i = 0.079 Re_g^{-0.25}\left(1 + 300\frac{\delta}{D}\right), \tag{A.10}$$

$$Re_g = \frac{\rho_g u_g D}{\mu_g}, \tag{A.11}$$

$$\Delta h_{eq} = \min[k_s, k_s\{2.136\log_{10}(Re_g) - 9.68\}], \tag{A.12}$$

$$k_s = 0.57\delta + 21.73 \times 10^3\delta^2 - 38.8 \times 10^6\delta^3 + 55.68 \times 10^9\delta^4, \tag{A.13}$$

It is assumed in calculating τ_{fg} that u_g is much larger than u_f. Also, assuming the liquid film is sufficiently thin and gravitational force acting on the film is negligible, δ is calculated by Eq. (8). The wall friction factor is given by

$$f_w = 0.079 Re_f^{-0.25}, \tag{A.14}$$

where the film Reynolds number is defined by

$$Re_f = \frac{\rho_l u_f D}{\mu_l}. \tag{A.15}$$

If the tentative value of E_∞ is used, δ can be iteratively solved from Eqs. (8), (A.11) and (A.14). Using the calculated δ, the amount of m_D and m_E are estimated from the above equations. Next, using Eq. (11), the value of E_∞ is updated. This procedure is repeated until convergence to obtain final value of E_∞.

Appendix B. Outline of the computer program, ANDRE

The computer program, ANDRE, uses the following conservation equations of mass and momentum based on a one-dimensional multi-fluid model [26]:

$$\frac{\partial}{\partial t}(\alpha_k\rho_k)+\frac{\partial}{\partial z}(\alpha_k\rho_k u_k^{n+1})=\sum_{p\neq k}(\Gamma_{pk}-\Gamma_{kp}), \tag{B.1}$$

$$\begin{aligned}&\alpha_k\rho_k\frac{\partial u_k}{\partial t}+\alpha_k\rho_k u_k\frac{\partial u_k}{\partial z}\\&\quad=-\alpha_k\left(\frac{\partial P}{\partial z}\right)^{n+1}+M_{\mathrm{w},k}^{n+1}+M_{\mathrm{i},k}^{n+1}-\alpha_k\rho_k g\\&\qquad+\sum_{p\neq k}\left\{\Gamma_{pk}\left(u_p^{n+1}-u_k^{n+1}\right)\right\},\end{aligned} \tag{B.2}$$

where t is the time, z the axial position, α the volume fraction, ρ the density, u the velocity, P the pressure, M_{w} the wall friction force, M_{i} the interfacial drag force and g the gravitational acceleration; the subscript k is the phase index and Γ_{12} represents the phase change rate from the phase 1 to the phase 2. The constitutive equations used for mathematically closing the basic Eqs. (B.1) and (B.2) are expressed in the following forms:

$$\sum_{p=1}^{m}\alpha_p=1, \tag{B.3}$$

$$M_{\mathrm{w},k}^{n+1}=-C_{\mathrm{w},k}u_k^{n+1}, \tag{B.4}$$

$$M_{\mathrm{i},k}^{n+1}=\sum_{p\neq k}M_{\mathrm{i},kp}^{n+1}=-\sum_{p\neq k}\left\{C_{\mathrm{i},kp}\left(u_k^{n+1}-u_p^{n+1}\right)\right\}, \tag{B.5}$$

where m denotes the number of phases.

The governing equations of the multi-fluid model (B.1)–(B.5) are discretized with the semi-implicit scheme on the staggered mesh. The term with the superscript $n+1$ in the equations are evaluated at the new time level $(n+1)\Delta t$, where Δt denotes the time step. Full donor cell differencing is used for the convection terms in Eqs. (B.1) and (B.2). In the solution scheme, the discretized form of momentum conservation equation (B.2) is arranged into

$$\sum_{p=1}^{m}a_{kp}u_p^{n+1}=\phi_k-\alpha_k\left(\frac{\partial P}{\partial z}\right)^{n+1}. \tag{B.6}$$

Since the number of momentum equations is m ($k=1$–m), the velocity of phase k at new time level is expressed as

$$u_k^{n+1}=b_k+c_k\left(\frac{\partial P}{\partial z}\right)^{n+1}. \tag{B.7}$$

Substituting this equation into the mass conservation Eqs. (B.1) and (B.3), the following nonlinear algebraic equations about P^{n+1} and α^{n+1} are obtained:

$$f_k(P^{n+1},\alpha_k^{n+1})=0, \tag{B.8}$$

$$f_{m+1}=\sum_{p=1}^{m}\alpha_p^{n+1}=1. \tag{B.9}$$

Applying the Newton–Raphson method to these equations, the Jacobi equation in the following form is obtained:

$$\tilde{A}_{\mathrm{NR}}^{n'}\begin{bmatrix}\delta P\\ \delta\alpha_1\\ \vdots\\ \delta\alpha_m\end{bmatrix}_j^{n'}+\tilde{B}_{\mathrm{NR}}^{n'}\begin{bmatrix}\delta P_{j-1}\\ \delta P_j\\ \delta P_{j+1}\end{bmatrix}^{n'}=\vec{F}_{\mathrm{NR}}^{n'}, \tag{B.10}$$

where n' is the number of iteration in the Newton–Raphson method and j denotes the discrete position: $z=j\Delta z$ (Δz is the mesh size). This equation is further transformed to

$$\begin{bmatrix}\delta P\\ \delta\alpha_1\\ \vdots\\ \delta\alpha_m\end{bmatrix}_j^{n'}+(\tilde{A}_j^{n'})^{-1}\tilde{B}_j^{n'}\begin{bmatrix}\delta P_{j-1}\\ \delta P_j\\ \delta P_{j+1}\end{bmatrix}^{n'}=(\tilde{A}_j^{n'})^{-1}\vec{F}_j^{n'}. \tag{B.11}$$

Extraction of the first line from this equation yields the tri-diagonal matrix about δP_j, which is solved with the tri-diagonal matrix algorithm. If δP is known, $\delta\alpha$ is calculated from Eq. (B.11). After the convergence of the Newton–Raphson method, pressure and volume fractions at the new time level are calculated by

$$P^{n+1}=P^{n'}+\delta P^{n'}, \tag{B.12}$$

$$\alpha_k^{n+1}=\alpha_k^{n'}+\delta\alpha_k^{n'}. \tag{B.13}$$

From these results, the new densities and velocities of all the phases are readily calculated with the equations of state and Eq. (B.7), respectively. This is the final step to obtain the solution at $(n+1)\Delta t$; the same procedure is repeated till $n\Delta t$ reaches prescribed time.

References

[1] M. Wicks III, A.E. Dukler, Entrainment and pressure drop in concurrent gas–liquid flow: air water in horizontal flow, AIChE J. 6 (3) (1960) 463–468.
[2] I.I. Paleev, B.S. Filippovich, Phenomena of liquid transfer in two-phase dispersed annular flow, Int. J. Heat Mass Transfer 9 (1966) 1089–1093.
[3] G.B. Wallis, Phenomena of liquid transfer in two-phase dispersed annular flow, Int. J. Heat Mass Transfer 11 (1968) 783–785.
[4] M. Ishii, K. Mishima, Droplet entrainment correlation in annular two-phase flow, Int. J. Heat Mass Transfer 32 (10) (1989) 1835–1846.
[5] A.H. Govan, G.F. Hewitt, D.G. Owen, T.R. Bott, An improved CHF modelling code, in: Proceedings of the Second UK National Heat Transfer Conference, 1988, pp. 33–48.
[6] S. Sugawara, Droplet deposition and entrainment modeling based on the three-fluid model, Nucl. Eng. Des. 122 (1990) 67–84.

[7] S. Sugawara, Ph.D. Thesis, Tokyo Institute of Technology, 1990 (see also).
[8] I. Kataoka, M. Ishii, A. Nakayama, Entrainment and deposition rates of droplets in annular two-phase flow, Int. J. Heat Mass Transfer 43 (2000) 1573–1589.
[9] G.F. Hewitt, N.S. Hall-Taylor, Annular Two-phase Flow, Pergamon, New York, 1970 (Chapter 8).
[10] M. Ishii, M.A. Grolmes, Inception criteria for droplet entrainment in two-phase concurrent film flow, AIChE J. 21 (2) (1975) 308–318.
[11] P.B. Whalley, G.F. Hewitt, The correlation of liquid entrainment fraction and entrainment rate in annular two-phase flow, UKAEA Report No. AERE-R9187, 1978.
[12] G.B. Wallis, One-dimensional Two-phase Flow, McGraw-Hill, New York, 1969 (Chapter 11).
[13] L.B. Cousins, W.H. Denton, G.F. Hewitt, Liquid mass transfer in annular two-phase flow, in: Proceedings of Symposium on Two-Phase Flow, Exeter, paper C4, 1965.
[14] L.B. Cousins, G.F. Hewitt, Liquid mass transfer in annular two-phase flow: droplet deposition and liquid entrainment, UKAEA Report No. AERE-R5657, 1968.
[15] G.F. Hewitt, D.J. Pulling, Liquid entrainment in adiabatic steam–water flow, UKAEA Report No. AERE-R5374, 1969.
[16] M. Yanai, Study on boiling heat transfer in a flow channel, Ph.D. Thesis, Kyoto University, 1971.
[17] J. Würtz, An experimental and theoretical investigation of annular steam–water flow in tube and annuli at 30 to 90 Bar, Riso Report No. 372, 1978.
[18] R.F.K. Keeys, J.C. Ralph, D.N. Roberts, Liquid entrainment in adiabatic steam–water flow at 500 and 1000 psia, UKAEA Report No. AERE-R6293, 1970.
[19] B.I. Nigmatulin, V.I. Malyshenko, Y.Z. Shugaev, Investigation of liquid distribution between the core and the film in annular dispersed flow of steam/water mixture, Teploenergetika 23 (5) (1976) 66–68.
[20] P.B. Whally, G.F. Hewitt, P. Hutchinson, Experimental wave and entrainment measurements in vertical annular two-phase flow, UKAEA Report No. AERE-R7521, 1973.
[21] K. Singh, C.C.St. Pierre, W.A. Cargo, E.O. Moeck, Liquid film flow rates in two-phase flow of steam and water at 1000 psia, AIChE J. 15 (1969) 51–56.
[22] A.W. Bennett, G.F. Hewitt, H.A. Kearsey, R.K.F. Keeys, D.J. Pulling, Studies of burnout in boiling heat transfer to water in round tubes with non-uniform heating, UKAEA Report No. AERE-R5076, 1966.
[23] D.G. Owen, G.F. Hewitt, T.R. Bott, Equilibrium annular flows at high mass fluxes; data and interpretation, PCH PhysicoChemical Hydrodynamics 6 (1/2) (1985) 115–131.
[24] J.C. Asali, Entrainment in vertical gas–liquid annular flows, Ph.D. Thesis, University of Illinois, 1983.
[25] J.G. Collier, G.F. Hewitt, Data on the vertical flow of air–water mixtures in the annular and dispersed flow regions, Part II: film thickness and entrainment data and analysis of pressure drop measurements, Trans. Inst. Chem. Eng. 39 (1961) 127–144.
[26] T. Okawa, T. Kitahara, K. Yoshida, T. Matsumoto, I. Kataoka, Numerical simulation of annular-dispersed flows in round tubes and annuli using a multi-fluid model, in: Proceedings of the Third UK–Japan Seminar on Multi-phase Flow and Nuclear Safety, 2000, pp. 1–6.